AIAA JOURNAL
Vol. 36, No. 11, November 1998

Bearing Failure in Pin Contact of Composite Laminates

P. S. Wu* and C. T. Sun†
Purdue University, West Lafayette, Indiana 47907-1282

A fiber-microbuckling-based failure model for contact between a pin and a composite laminate is reviewed. This failure model is employed to study the effects of various parameters on the bearing failure. The parameters considered include ply orientation, stacking sequence, laminate thickness, pin material, and clamping condition. Accompanying the analysis, pin contact experiments are conducted. The test results demonstrate the influence of these parameters on the contact bearing strength. They are also used to evaluate the model predictions. Several bearing failure mechanisms are found to be dependent on ply thickness and orientation. If the failure is dominated by fiber microbuckling, then the present model yields quite accurate predictions of bearing failure.

Introduction

MECHANICALLY fastened joints are commonly used in composite parts. To utilize the full potential of these materials as structural elements, the strength and failure behavior of bolted joints must be understood. Many studies on this topic have been reported.[1–14] A recent paper by Camanho and Mathews[15] gave an extensive review of the subject, listing nearly 100 publications up to 1996.

A large number of variables such as ply orientation, ply stacking sequence, pin material, pin diameter, laminate thickness, and lateral constraint can affect bearing strength. Collings[3] showed that bearing strength is affected by ply orientation. Quinn and Matthews[2] and Smith and Pascoe[6] reported that stacking sequence has a significant effect on bearing strength and may alter the failure mode. Chang et al.[4] used a two-dimensional finite element method for stress analysis and the Yamada–Sun[16] failure criterion for ultimate strength prediction. Subsequently, Chang et al.[5] extended the analysis to account for nonlinear elastic stress–strain behavior for shear and found improved predictions. Eriksson[7] observed that bearing strength increases slightly with increasing hole diameter or laminate thickness. It has been concluded that bearing strength is strongly affected by lateral constraint of the material surrounding the loaded hole.[7–9] Increasing the clamping force would increase the bearing strength. Hyer et al.[10] indicated that inclusion of pin elasticity increases the predicted load capacity slightly. Chang and Chang[11] developed a progressive damage model to predict tension and shear-out failures at loaded holes. Both geometric and material nonlinearity were considered. Recently, Wang et al.[13] and Hung and Chang[14] reported a further experimental study, together with a modeling effort in bearing failure of bolted composite joints. A semicircular notched specimen was used to investigate the bearing failure. Damage modes and the effect of lateral supports on bearing strength were carefully studied. However, the model was restricted to two dimensions.

The failure process in a bolted composite joint is very complicated. Most of the earlier work employed two-dimensional models with linear or nonlinear material properties. Classical failure criteria or their modified versions were used to predict in-plane failure of the laminate. Obviously, these two-dimensional models cannot account for three-dimensional effects such as the effects of stacking sequence, clamping pressure, etc.

Recently, Sun and Wu[17] simulated the bearing failure in a bolted composite joint with a hard steel pin in contact with a straight-edged laminate (see Fig. 1). They found that the out-of-plane shear stress plays an important role in the initiation of contact failure. They observed that contact failure occurred first in the 0-deg plies near the free surfaces of the laminate in the form of fiber microbuckling or kinking, as shown in Fig. 2. Upon increasing the contact force, the kink band produced by microbuckling propagated toward the midplane of the laminate, as shown in Fig. 3. The corresponding pin load-displacement curve is shown in Fig. 4. Initiation of contact failure was noted to have taken place at about 80% of the peak load, depending on the layup of the laminate.

Sun and Wu[17] adopted a microbuckling model proposed by Sun and Jun[18] to analyze the pin contact failure initiation load in cross-ply AS4/3501-6 laminates. The predictions were fairly good compared with the test results. In the microbuckling analysis, three-dimensional stresses near the contact region are needed. Moreover, the nonlinear stress–strain behavior of the composite must be modeled.

In this study, experiments are conducted to investigate the effects of ply orientation, stacking sequence, pin material, laminate thickness, and lateral clamping pressure on the initiation and ultimate bearing failure loads of pin contact. The methodology of Sun and Wu[17] is used to predict the failure initiation load.

Failure Prediction Method

Composite Plasticity Model

To model the nonlinear behavior of the composite, Sun and Wu[17] adopted the three-dimensional plastic potential

$$f(\sigma_{ij}) = \tfrac{1}{2}\left[(\sigma_{22}-\sigma_{33})^2 + 4\sigma_{23}^2 + 2a_{66}\left(\sigma_{12}^2+\sigma_{13}^2\right)\right] \qquad (1)$$

where a_{66} is a coefficient representing the initial orthotropy in plasticity. From this plastic potential, the plastic strain increment can be obtained, i.e.,

$$\mathrm{d}\varepsilon_{ij}^{p} = \frac{\partial f}{\partial \sigma_{ij}}\,\mathrm{d}\lambda \qquad (2)$$

in which $\mathrm{d}\lambda$ is a proportionality factor. Note that the use of the plastic potential given by Eq. (1) implies that there is no plastic strain in the fiber direction and that the composite is transversely isotropic.

The value of a_{66} can be determined from the uniaxial stress–strain curves of off-axis composite specimens.[19] For AS4/3501-6 carbon/epoxy composite, $a_{66} = 2.5$. By using the concept of effective stress defined as $\bar{\sigma} = \sqrt{(3f)}$ and the corresponding effective plastic strain increment $\mathrm{d}\bar{\varepsilon}^{p}$, the proportionality factor $\mathrm{d}\lambda$ can be expressed as[19]

$$\mathrm{d}\lambda = \frac{3}{2}\frac{\mathrm{d}\bar{\varepsilon}^{p}}{\mathrm{d}\bar{\sigma}}\frac{\mathrm{d}\bar{\sigma}}{\bar{\sigma}} \qquad (3)$$

For AS4/3501-6, the relation between $\bar{\sigma}$ and $\bar{\varepsilon}^{p}$ is given by a power law as

$$\bar{\varepsilon}^{p} = A(\bar{\sigma})^{n}, \qquad A = 1.05\times 10^{-15}\ (\mathrm{MPa}), \qquad n = 5.2 \qquad (4)$$

Microbuckling Model

It is well known that compressive failure in polymeric matrix composites often takes the form of fiber microbuckling. A fiber-microbuckling model proposed by Sun and Jun[18] was adapted

Presented as Paper 97-1119 at the AIAA/ASME/ASCE/AHS/ASC 35th Structures, Structural Dynamics, and Materials Conference, Kissimmee, FL, April 7–10, 1997; received Sept. 12, 1997; revision received June 8, 1998; accepted for publication July 4, 1998.

*Graduate Student, School of Aeronautics and Astronautics; currently Aeronautical Engineer, Aeronautical Research Laboratory, Taichung 40227, Taiwan, Republic of China.

†Professor, School of Aeronautics and Astronautics. Fellow AIAA.

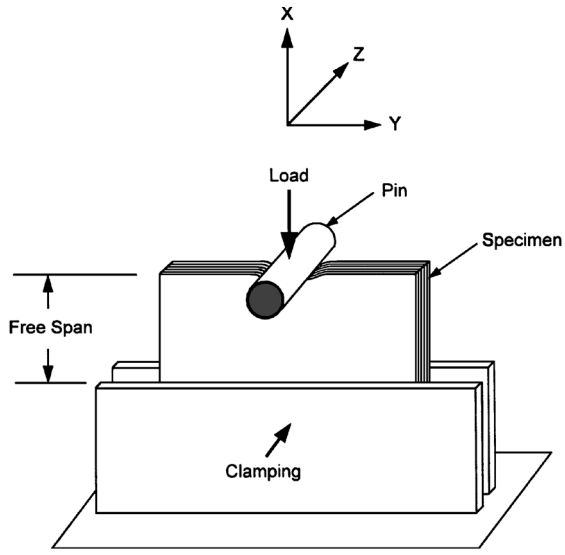

Fig. 1 Schematic of pin contact with a straight-edged laminate.

Fig. 2 Micrograph (cross-sectional view) in 0-deg plies in $[0/90]_{10S}$ laminate produced by pin contact.

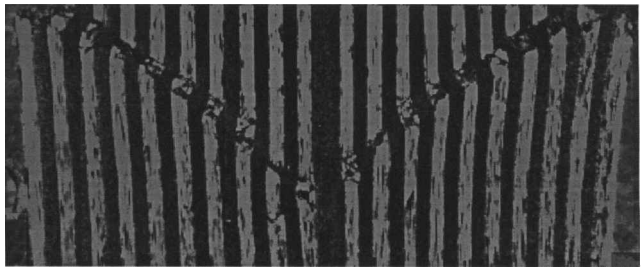

Fig. 3 Photograph of the damage in the cross section of $[0/90]_{10S}$ laminate loaded beyond the peak contact load.

by Sun and Wu[17] to predict contact failure initiation with a fairly good result. This model predicts the microbuckling stress (compressive strength) of a fiber composite to be

$$(\sigma_{xx})_{\text{cr}} = G_m^{\text{ep}} / (1 - c_f) \tag{5}$$

where c_f is the fiber volume fraction and G_m^{ep} is the matrix elastic–plastic shear modulus given by

$$G_m^{\text{ep}} = \left[\frac{1}{G_m} + \frac{9\theta^2}{(\beta^2 + 3\theta^2) H_p} \right]^{-1} \tag{6}$$

In Eq. (6), G_m is the matrix elastic shear modulus, H_p is the plastic modulus of the matrix, θ is the fiber misalignment angle, and

$$\beta = \frac{1}{\alpha c_f + c_m}, \qquad \alpha = \frac{E_f}{E_{\text{ms}}} \tag{7}$$

where E_f is the fiber modulus of elasticity, E_{ms} is the matrix secant modulus, and c_m is the matrix volume fraction.

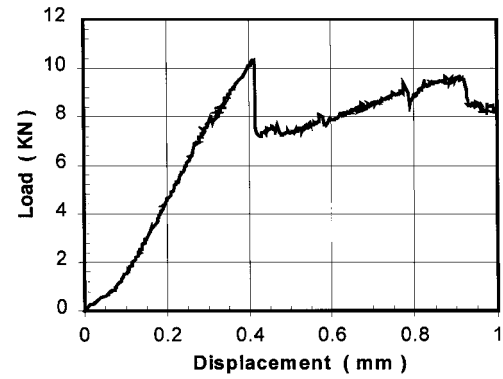

Fig. 4 Typical load-displacement curve for a cross-ply laminate.

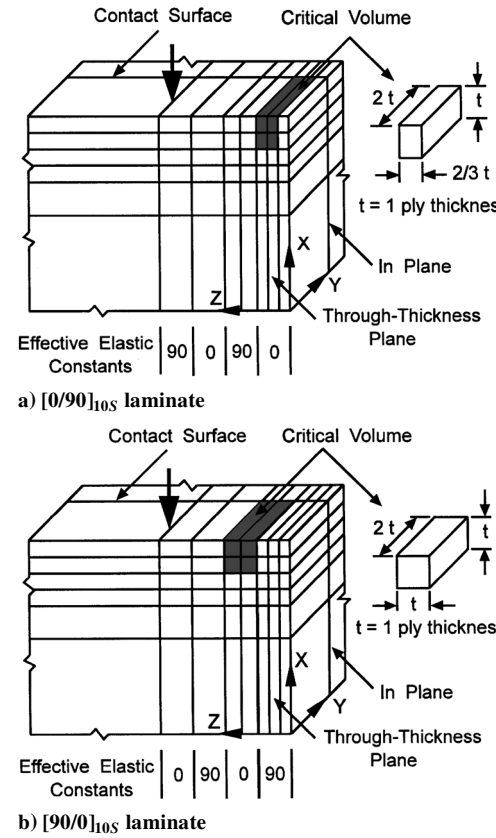

Fig. 5 Schematic showing the location and size of critical volume for contact damage initiation near the edge contact surface.

Assume that fiber buckling occurs in the x–z plane; then $\tau_{xz} = \sigma_{xx}\theta$. In the present application, θ should be interpreted as the ratio of the out-of-plane shear stress τ_{xz} and the normal stress σ_{xx}, i.e., $\theta = \tau_{xz}/\sigma_{xx}$.

The plastic modulus of the matrix H_p depends on the applied stress σ_{xx}. The buckling stress $(\sigma_{xx})_{\text{cr}}$ is obtained by finding the value of σ_{xx} that satisfies Eq. (5). The numerical procedure for the solution can be found in Ref. 18.

Essential to this analysis is the complete nonlinear stress–strain curve of the matrix. For the 3501-6 epoxy matrix, the uniaxial stress–strain curves for various temperatures were given by Crasto and Kim.[20]

Pin Contact Failure Initiation Prediction

The stress distribution in the laminate produced by pin contact is nonuniform. In fact, significant stress concentrations are found near the free surfaces of the laminate where failure usually initiates. Thus, the first 0-deg ply from the free surface is to be considered for failure analysis.

By assuming that fiber microbuckling should occur simultaneously in a finite volume, a critical volume in the stress concentration site in this 0-deg ply is taken for analysis. Figure 5 shows the

critical volumes for 0-deg plies at the free surface and inside the free surface, respectively. For the 0-deg ply at the free surface, a layer of one-third ply thickness is excluded from the critical volume to avoid the inaccuracy of the finite element analysis due to the traction free-boundary condition. For the interior 0-deg ply, the entire ply thickness is included in the critical volume. As indicated in Fig. 5, the x and y dimensions of the critical volumes are t and $4t$, respectively, where t is ply thickness. These suggested critical volumes are found to yield good predictions.[21]

The average normal stress σ_{xx} and out-of-plane shear stress τ_{xz} in the critical volume are obtained from the three-dimensional elastic–plastic finite element analysis. These stresses are then used to determine microbuckling stress with the aid of Eq. (5).

In this study, the commercial finite element code ABAQUS is used to perform the elastic–plastic pin contact analysis. The nonpenetration condition at the contact region is imposed through the use of interface elements. For the contact surfaces, it is assumed that the pin and the laminate stick in the z direction, whereas sliding was assumed for the x and y displacements. These assumptions imply that contact friction prevents sliding between the contact surfaces only in the thickness direction.

Experimental Results and Predictions

The schematic of the setup for the pin contact test is shown in Fig. 1. Laminate specimens of AS4/3501-6 composite are approximately 50 mm (in the x direction) × 45 mm. The contact edge of the laminate is polished with 600-grit sandpaper to ensure a flat and smooth contact surface. To avoid global buckling, the specimen is clamped, leaving a 10-mm free span. The diameter of the loading pin is 12.7 mm. Loading is applied using an MTS servohydraulic machine at a stroke rate of 0.1 mm/min. Load-deflection curves are recorded. Unless specified otherwise, the pin used is hardened steel.

Six replicas are tested beyond their peak bearing loads. Additional specimens are used to determine the failure initiation load. Typically, a specimen is loaded to 90% of the ultimate bearing load and is subsequently unloaded and sectioned along the contact centerline. The cross section is examined with a microscope. If damage is detected, then another specimen is loaded to 87.5% of ultimate load and then sectioned for inspection. This procedure is repeated using incrementally smaller loading until no damage is found. The accuracy in determining damage initiation load using this procedure should be within about 2.5%.

Stacking Sequence and Percentage of 0-Degree Plies

Five 40-ply laminates are studied, i.e., $[0/90/\pm45]_{5S}$, $[90/0/\pm45]_{5S}$, $[0/90]_{10S}$, $[90/0]_{10S}$, and $[0]_{40}$. These laminates contain 25%, 50%, and 100% 0-deg plies, respectively. The tested ultimate contact load, damage initiation load, and predicted damage initiation load are listed in Table 1. It is evident that failure does not initiate at the same percentile of ultimate load for these layups. In general, the higher the percentage of 0-deg plies in the laminate, the larger the initial and ultimate failure loads. However, the initial and ultimate failure loads are not in proportion to the percentage of 0-deg plies.

The microphotograph of the cross section near the free surface in the $[90/0/\pm45]_{5S}$ laminate loaded beyond peak load is shown in Fig. 6. The distinct kink bands observed in the $[0/90]_{10S}$ and $[90/0]_{10S}$ laminates (see Fig. 3) are not observed here. However, the initial contact failure still occurred in the outermost 0-deg ply. The failure onset mechanisms of the quasi-isotropic and cross-ply laminates appear to be the same, but the damage propagation mechanisms could be different.

The test results indicate that $[90/0]_{10S}$ and $[0/90]_{10S}$ laminates have almost identical bearing strengths. The same can be said about the $[0/90/\pm45]_{5S}$ and $[90/0/\pm45]_{5S}$ laminates. For laminates with many repeating sublaminates, the stacking sequence does not seem to affect their bearing strength. The failure mode of the unidirectional laminate $[0]_{40}$ appears somewhat different from that of the cross-ply laminates due to the low transverse strength of the composite. Figure 7 shows the microphotograph of the contact surface in the $[0]_{40}$ specimen loaded beyond ultimate contact load. It is evident that matrix cracking (splitting) extends along the thickness direction. The cross-sectional view, shown in Fig. 8, indicates that the kink bands similar to those in the cross ply laminates are also present in the $[0]_{40}$ laminate.

Table 1 Effect of stacking sequence and percentage of 0-deg plies on contact failure

Laminate	Ultimate load, kN	Damage initiation load, kN		
		% of ultimate load	Experiment	Prediction
$[0]_{40}$	11.3 ± 0.7	80	9.0	12.7
$[0/90]_{10S}$	10.2 ± 0.6	77.5	7.9	8.0
$[90/0]_{10S}$	10.5 ± 0.6	77.5	8.1	8.2
$[0/90/\pm45]_{5S}$	8.2 ± 0.3	70	5.7	5.4
$[90/0/\pm45]_{5S}$	8.0 ± 0.3	70	5.6	5.5

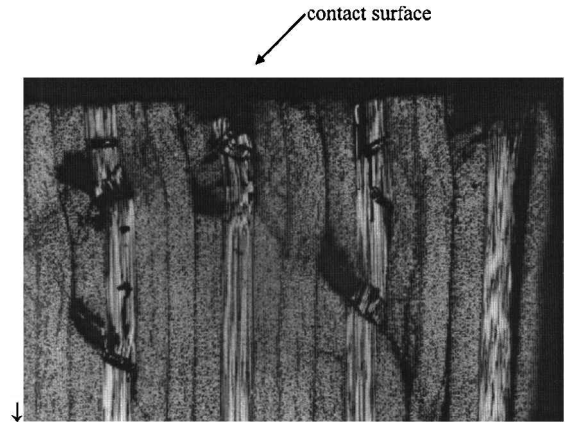

Fig. 6 Cross-sectional view (40×) showing contact damage to ultimate contact.

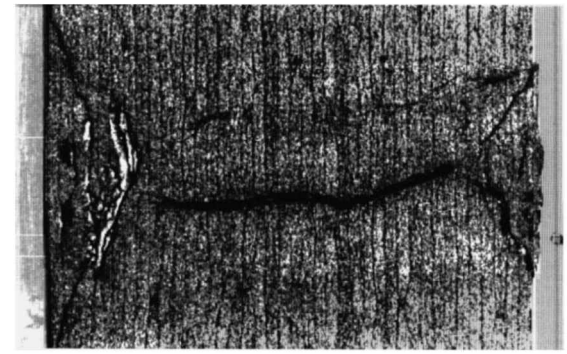

Fig. 7 Top view (20×) of contact surface near the free surface in $[90/0/\pm45]_{5S}$ laminate showing damage in $[0]_{40}$ laminate loaded to ultimate contact load.

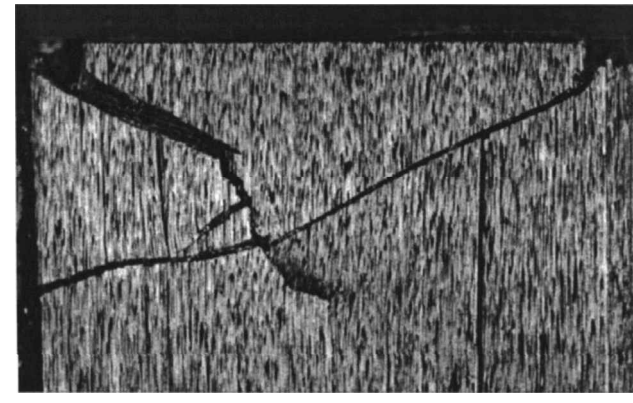

Fig. 8 Cross-sectional view (20×) showing damage in $[0]_{40}$ laminate loaded to ultimate contact load AS4/3501-6 composite.

Table 2 Compressive in-plane transverse σ_{yy} and thickness normal σ_{zz} stresses within the critical volume of laminates loaded at their respective damage initiation loads

Laminate	σ_{yy}, MPa	σ_{zz}, MPa
$[0]_{40}$	247	122
$[0/15/0/-15]_{5S}$	240	85
$[0/30/0/-30]_{5S}$	225	80
$[0/45/0/-45]_{5S}$	195	73
$[0/90]_{10S}$	165	66

Table 3 Ultimate and damage initiation loads for $[0/\theta/0/-\theta]_{5S}$-type laminates

		Damage initiation load, kN		
Laminate $[0/\theta/0/-\theta]_{5S}$	Ultimate load, kN	% of ultimate load	Experiment	Prediction
$[0]_{40}$	11.3 ± 0.7	80	9.0	12.7
$[0/15/0/-15]_{5S}$	9.7 ± 0.8	77.5	7.5	11.3
$[0/30/0/-30]_{5S}$	10.2 ± 0.6	77.5	7.9	8.4
$[0/45/0/-45]_{5S}$	9.8 ± 0.5	77.5	7.6	7.4
$[0/90]_{10S}$	10.2 ± 0.6	77.5	7.9	8.0

The sequence of occurrence of these two failure modes (splitting and microbuckling) can be determined from the three-dimensional stress analysis result. Table 2 presents compressive stresses σ_{yy} and σ_{zz} in the critical volume in a number of laminates at their respective damage initiation loads. In the $[0]_{40}$ laminate, the in-plane transverse stress σ_{yy} is significantly higher than the compressive strength of 228 MPa for AS4/3501-6 composite.[22] Hence, in the $[0]_{40}$ laminate, splitting would occur before fiber microbuckling. This explains why the predicted damage initiation load in the $[0]_{40}$ laminate in the microbuckling model is much higher than the test data.

It is interesting to note that the ultimate bearing strength of the $[0]_{40}$ laminate is merely 10% higher than that of the cross-ply laminates even though they contain twice the number of 0-deg plies.

Ply Orientation

Laminates of the type $[0/\theta/0/-\theta]_{5S}$ ($\theta = 0, 15, 30, 45$, and 90 deg) are investigated to understand the effect of ply orientation on contact failure. For these laminates, the experimental data and the predictions of damage initiation are listed in Table 3. It is noted that all of the laminates sustain similar ultimate contact loads.

From Table 2, it can be seen that the in-plane compressive transverse normal stress σ_{yy} in the critical volume in the $[0/15/0/-15]_{5S}$ laminate also exceeds the transverse compressive strength of the composite. The microscopic inspection of the contact surface confirms that transverse matrix cracking (splitting) occurs before fiber microbuckling. The failure mode in the $[0/30/0/-30]_{5S}$ and $[0/45/0/-45]_{5S}$ laminates appears quite similar to that of the $[0/90]_{10S}$ laminate, and fiber microbuckling is the only failure mode at the damage initiation stage. Accordingly, predictions of their failure initiation loads generally agree with the experimental data.

It is interesting to note that the experimental contact strength of the $[0/45/0-45]_{5S}$ laminate is lower than that of the $[0/90]_{10S}$ laminate. This phenomenon was also observed by Collings.[3] Intuitively, one would expect that the 45-deg plies would carry more load than the 90-deg plies, and consequently, the $[0/45/0/-45]_{5S}$ laminate should have a higher bearing strength than the $[0/90]_{10S}$. This phenomenon cannot be explained by linear elasticity theory; nonlinear constitutive models of the composite must be invoked.

Figure 9 shows the nonlinear stress–strain curves for a number of off-axis AS4/3501-6 composite specimens. Comparing the stress–strain curves for the 45- and 90-deg specimens, we note that they cross each other at about 2% strain. This implies that at strains larger than 2%, the 90-deg ply can carry more load than the 45-deg ply. According to the result of the elastic–plastic analysis, the normal strain in the loading direction at the failure load could exceed 4%.

Table 4 Material properties of pins

Pin	Material constants			
Hard steel	$E = 200$ GPa,	$\sigma_y = 1380$ MPa,	$\sigma_u = 1450$ MPa,	$\nu = 0.3$
Soft steel	$E = 200$ GPa,	$\sigma_y = 350$ MPa,	$\sigma_u = 500$ MPa,	$\nu = 0.3$
Aluminum	$E = 69$ GPa,	$\sigma_y = 255$ MPa,	$\sigma_u = 290$ MPa,	$\nu = 0.3$

Table 5 Ultimate and damage initiation loads of laminates for pins of different materials

		Damage initiation load, kN		
Pin	Ultimate load, kN	% of ultimate load	Experiment	Prediction
		$[0/90]_{10S}$ laminate		
Hard steel	10.2 ± 0.6	77.5	7.9	8.0
Soft steel	10.9 ± 0.5	77.5	8.4	8.3
Aluminum	23.0 ± 0.6	70	16.1	13.0
		$[90/0]_{10S}$ laminate		
Hard steel	10.5 ± 0.4	77.5	8.1	8.2
Soft steel	11.3 ± 0.4	77.5	8.8	8.4
Aluminum	23.6 ± 1.2	70	16.5	13.2

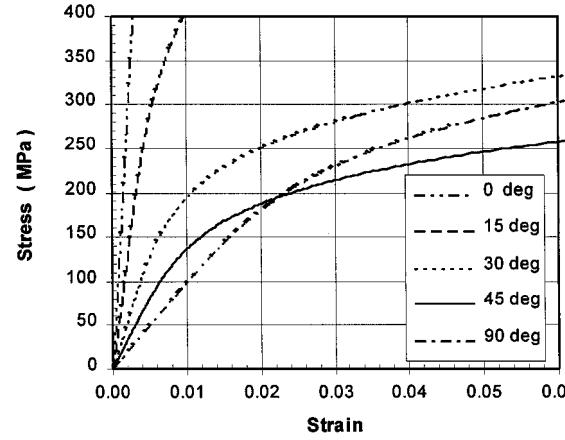

Fig. 9 Off-axis stress–strain curves for AS4/3501-6.

Effect of Pin Material

In aircraft structures, pins made of alloys such as steel, titanium, and aluminum are used. In this study, pins made of three different materials, including hard steel, soft steel, and aluminum, are used. Their mechanical properties are listed in Table 4. The pin contact experimental data and numerical predictions are presented in Table 5. The results indicate that a softer pin (of lower yield stress) would produce a higher bearing strength. The aluminum pin yields very high failure loads but also deforms severely during the contact process. However, the contact failure mechanism in the composite laminate is found to be identical for the three different pins.

The predictions of failure initiation loads for both hard and soft steel pins are quite accurate compared with the test results. For the aluminum pin, the predictions are significantly lower than the test data. This could result from the use of the simplifying assumptions in the analysis, which may be inadequate to simulate the large deformation experienced by the aluminum pin.

Laminate Thickness

To investigate the thickness effect on the bearing strength of composites, cross-ply laminates of three different thicknesses, i.e., 2.56 mm (20 plies), 5.12 mm (40 plies) and 7.68 mm (60 plies), are tested. Experimental and predicted contact failure loads are presented in Fig. 10. The normalized line load is the contact load divided by the laminate thickness. It is evident that the normalized damage initiation load is nearly constant with respect to laminate thickness. However, the normalized ultimate load increases as the laminate thickness increases. In other words, the total bearing load increases faster than the laminate thickness. This phenomenon has been reported but not explained in the literature on composite joint

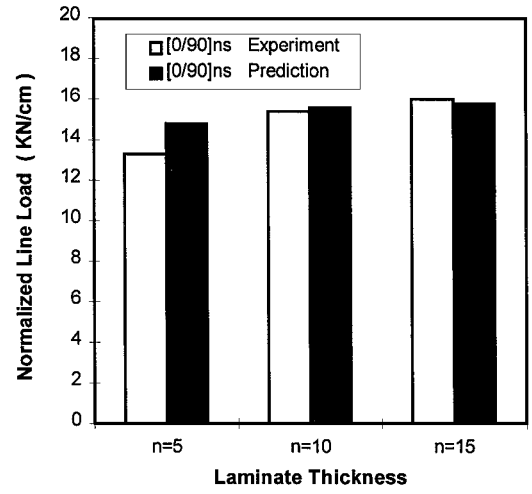

a) Damage initiation

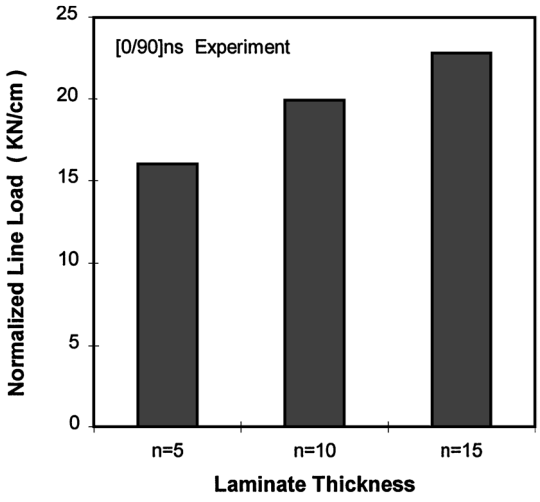

b) Ultimate failure

Fig. 10 Normalized contact loads for $[0/90]_{nS}$ laminates of different thicknesses.

problems.[4,9] Referring to Fig. 3, we note that, in a thicker laminate, the kink bands that initiate near the two free surfaces of the laminate must propagate a greater distance to meet and cause the contact load to drop. Thus, thicker laminates are more efficient in taking contact loads.

Effect of Clamping

Lateral clamping on the laminate is found to greatly affect the bearing strength of bolted joints and has attracted extensive studies.[7–14] It has been found that bearing strength increases with the increase in clamping pressure. However, no analytical model has been developed to quantify this effect.

Lateral clamps reduce the out-of-plane displacement under pin contact and, as a result, also reduce the out-of-plane (interlaminar) shear stress σ_{xz}. In this research, the clamping effect is investigated by changing the free-span length S, which is the distance between the clamp and the contact edge of the laminate. The chosen lengths are 0.5, 3, and 10 mm, respectively.

The load-displacement curve for the $[90/0]_{15S}$ laminate with a free span of 3 mm is presented in Fig. 11. This curve is similar to that shown in Fig. 4 for a 10-mm free span. For the specimen with a 0.5-mm free span, as shown in Fig. 12, the laminate can carry additional loads after passing the first peak load. Experimental data and predictions are listed in Table 6.

In the three-dimensional finite element model, the z-direction displacement at every node on the laminate surface in the clamped area is assumed to be zero. This assumption seems to be adequate, as the predicted damage initiation loads agree quite well with the test data.

Table 6 Ultimate and damage initiation loads of laminates with different free spans S

Free-span length S, mm	Ultimate load, kN	Damage initiation load, kN: % of ultimate load	Damage initiation load, kN: Experiment	Damage initiation load, kN: Prediction
	$[90/0]_{10S}$ *laminate*			
0.5	12.0 ± 1.0	77.5	9.3	9.7
3.0	10.7 ± 0.4	77.5	8.3	8.3
10	10.5 ± 0.4	77.5	8.1	8.2
	$[90/0]_{15S}$ *laminate*			
0.5	20.2 ± 1.6	70	14.2	15.0
3.0	18.6 ± 1.0	70	13.0	12.5
10	17.9 ± 0.8	70	12.5	12.2

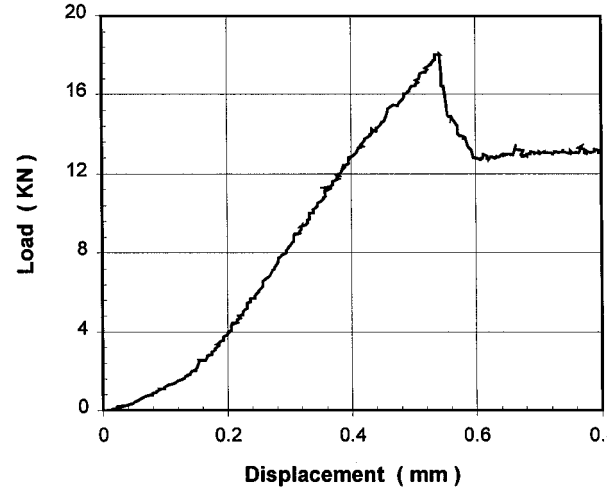

Fig. 11 Typical load-displacement curve of $[0/90]_{15S}$ laminate with 3-mm free span.

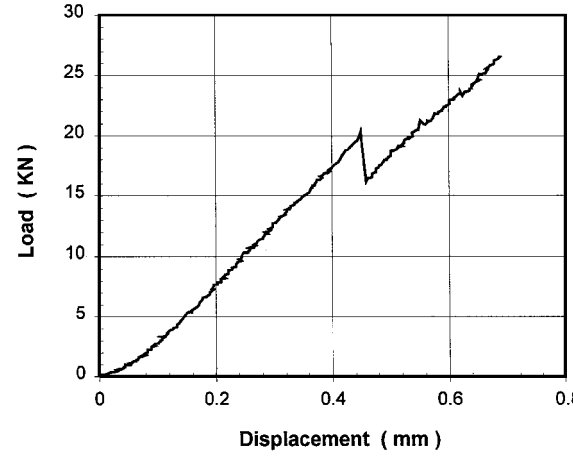

Fig. 12 Typical load-displacement curve of $[0/90]_{15S}$ laminate with 0.5-mm free span.

From the results presented in Table 6, it is seen that, to realize the benefit of lateral clamping, the clamp must be placed very close to the contact surface. The closeness to the contact surface is measured in terms of the ratio between the free span S and the laminate thickness. This explains why, for the same free span of 0.5 mm, the clamping effect on the thicker $[90/0]_{15S}$ laminate is much greater than that in the thinner $[90/0]_{10S}$ laminate.

Conclusions

In most composite laminates considered, fiber microbuckling appears to be the dominant mode of failure in the pin contact problem. In the prediction of contact failure, three-dimensional stress analyses must be performed using nonlinear constitutive models for the composite. It is found that the out-of-plane shear stress plays

an important role in the onset of microbuckling. Two-dimensional models are inadequate for this type of failure analysis.

Pin contact failure can be affected by many variables. The following is a summary of the major results of interest:

1) The ultimate contact load is not in proportion to the percentage of 0-deg plies in the laminate. Increasing the percentage of 0-deg plies may not result in an appreciable increase in bearing strength.

2) For laminates with many repeating sublaminates, stacking sequence has little effect on the contact failure load of the laminate.

3) Clusters of 0-deg plies such as $[0]_{40}$ can induce longitudinal fiber splitting before fiber microbuckling. The same can be said about laminates with small off-axis angles, such as $[0/15/0/-15]_{5S}$.

4) Greater laminate thicknesses increase the efficiency of contact load bearing of laminates.

5) Pins of lower yield stresses yield higher contact failure loads for the laminate and larger plastic deformations in the pin.

6) Lateral clamping is effective in improving bearing strength only when the clamps are placed very close to the contact surface.

Acknowledgments

This work was supported by the Office of Naval Research through Grant N00014-96-1-0822 to Purdue University. Y. D. S. Rajapakse was the Technical Monitor.

References

[1]Waszczak, J. P., and Cruse, T. A., "Failure Mode of Strength Predictions of Anisotropic Bolt Bearing Specimens," *Journal of Composite Materials*, Vol. 5, 1971, pp. 421–425.

[2]Quinn, W. J., and Matthews, F. L., "The Effect of Stacking Sequence of the Pin-Bearing in Glass Fiber Reinforced Plastic," *Journal of Composite Materials*, Vol. 11, 1977, pp. 139–145.

[3]Collings, T. A., "On the Bearing Strengths of CFRP Laminates," *Composites*, Vol. 13, 1982, pp. 241–252.

[4]Chang, F. K., Scott, R. A., and Springer, G. S., "Failure of Composite Laminates Containing a Pin Loaded Hole—Method of Solution," *Journal of Composite Materials*, Vol. 18, 1984, pp. 255–271.

[5]Chang, F. K., Scott, R. A., and Springer, G. S., "Failure Strength of Nonlinear Elastic Composite Laminates Containing a Pin Loaded Hole," *Journal of Composite Materials*, Vol. 18, 1984, pp. 464–477.

[6]Smith, P. A., and Pascoe, K. J., "The Effect of Stacking Sequence on the Bearing Strengths of Quasi-Isotropic Composite Laminates," *Composite Structures*, Vol. 6, 1986, pp. 1–20.

[7]Eriksson, L. I., "On the Bearing Strength of Bolted Graphite/Epoxy Laminates," *Journal of Composite Materials*, Vol. 24, 1990, pp. 1246–1269.

[8]Kretsis, G., and Matthews, F. L., "The Strength of Bolted Joints in Glass Fiber/Epoxy Laminate," *Composites*, Vol. 16, 1985, pp. 92–102.

[9]Tsujimoto, Y., and Wilson, D., "Elasto-Plastic Failure Analysis of Composite Bolted Joints," *Journal of Composite Materials*, Vol. 20, 1986, pp. 236–252.

[10]Hyer, M. W., Klang, E. C., and Cooper, D. E., "The Effect of Pin Elasticity, Clearance and Friction on the Stresses in a Pin-Loaded Orthotropic Plate," *Journal of Composite Materials*, Vol. 21, 1987, pp. 190–206.

[11]Chang, F. K., and Chang, K. Y., "Progressive Damage Model for Laminated Composites Containing Stress Concentrations," *Journal of Composite Materials*, Vol. 21, 1987, pp. 834–855.

[12]Graham, U., Wisnom, M. R., and Webber, P. H., "A Novel Finite Element Investigation of the Effects of Washer Friction in Composite Plates with Bolt-Filled Holes," *Composite Structures*, Vol. 29, 1994, pp. 329–339.

[13]Wang, H.-S., Hung, C.-L., and Chang, F. K., "Bearing Failure of Bolted Composite Joints. Part I: Experimental Characterization," *Journal of Composite Materials*, Vol. 30, No. 12, 1996, pp. 1284–1313.

[14]Hung, C.-L., and Chang, F. K., "Bearing Failure of Bolted Composite Joints. Part II: Model and Verification," *Journal of Composite Materials*, Vol. 30, No. 12, 1996, pp. 1359–1400.

[15]Camanho, P. P., and Mathews, F. L., "Stress Analysis and Strength Prediction of Mechanically Fastened Joints in FRP: A Review," *Composites Part A*, Vol. 28A, 1997, pp. 529–547.

[16]Yamada, S. E., and Sun, C. T., "Analysis of Laminate Strength and Its Distribution," *Journal of Composite Materials*, Vol. 12, 1978, pp. 275–284.

[17]Sun, C. T., and Wu, P. S., "Pin Contact Failure in Composite Laminates," *Proceedings of the Tenth International Conference on Composite Materials (ICCM X)* (Whistler, BC, Canada), Vol. 3, Woodhead Publishing, 1995, pp. 637–644.

[18]Sun, C. T., and Jun, A. W., "Compressive Strength of Unidirectional Fiber Composites with Matrix Non-Linearity," *Composite Science and Technology*, Vol. 52, 1994, pp. 577–587.

[19]Sun, C. T., and Chen, J. L., "A Simple Flow Rule for Characterizing Nonlinear Behaviors of Fiber Composites," *Journal of Composite Materials*, Vol. 23, 1989, pp. 1009–1020.

[20]Crasto, A. S., and Kim, R. Y., "The Effects of Constituent Properties on the Compression Strength of Advanced Composites," American Society for Testing and Materials Symposium on Compression Response of Composite Structures, Miami, FL, 1992.

[21]Wu, P. S., and Sun, C. T., "Modeling Bearing Failure Initiation in Pin-Contact of Composite Laminates," *Mechanics of Materials* (to be published).

[22]Daniel, I. M., and Ishai, O., *Engineering Mechanics of Composite Materials*, Oxford Univ. Press, New York, 1994.

A. M. Waas
Associate Editor